Chemical Science

ROYAL SOCIETY OF CHEMISTRY

EDGE ARTICLE

View Article Online
View Journal | View Issue

Cite this: *Chem. Sci.*, 2024, **15**, 220

All publication charges for this article have been paid for by the Royal Society of Chemistry

Received 8th October 2023
Accepted 28th November 2023

DOI: 10.1039/d3sc05318k

rsc.li/chemical-science

A salt-concentrated electrolyte for aqueous ammonium-ion hybrid batteries†

Jianming Meng,[a] Yu Song, *[ab] Jing Wang, *[d] Peng Hei,[a] Chang Liu,[a] Mengxue Li,[a] Yulai Lin[a] and Xiao-Xia Liu *[abc]

The development of aqueous ammonium-ion batteries (AAIBs) is currently attracting great attention because of the interesting electrochemical features induced by the charge carrier NH_4^+. One possible way to improve the performance of AAIBs is increasing the salt concentration in the electrolyte. Yet, few studies focus on the complex electrode–electrolyte interface behaviors in highly concentrated electrolytes, which affect the electrochemical performance of AAIBs significantly. Herein, we aim to understand the impact of CH_3COONH_4 electrolyte concentration on the NH_4^+ storage performance of a bimetallic hydroxide material. Experimental and theoretical simulation results indicate that the acetate anion will participate in the construction of the solvated NH_4^+ in a highly concentrated electrolyte, facilitating the adsorption of the solvated NH_4^+ cluster on the electrode surface. Besides, a new partial de-solvation model is also proposed, demonstrating an energy favorable de-solvation process. Finally, an ammonium-ion hybrid battery is designed, which provides a high average discharge voltage of 1.7 V and good energy density of 368 W h $kg_{(cathode)}^{-1}$, outperforming most of the state-of-the-art aqueous batteries. This work provides new understanding about the electrode's interfacial chemistry in different concentrated CH_3COONH_4 electrolytes, establishes a correlation between the electrolyte concentration and the electrode's performances, and demonstrates the superiority of the hybrid ammonium-ion battery design.

Introduction

Aqueous ammonium-ion batteries (AAIBs) using non-metallic ammonium ions (NH_4^+) as charge carriers are receiving increasing attention, due to the fast diffusion kinetics of NH_4^+ and the interesting H-bonding chemistry between NH_4^+ and host materials.[1–4] Current research in AAIBs mainly focuses on fabricating high-performance electrode materials, such as metal oxides,[5–9] polyanionic compounds,[10] conducting polymers,[11,12] Prussian blue analogues,[13–16] *etc.* Yet, the systematic study of electrolytes which are compatible with these NH_4^+ hosting materials is still lagging, limiting the development of competitive AAIBs.

A recent breakthrough in electrolyte engineering is achieved by simply increasing the salt concentration in aqueous solution, offering distinct merits over dilute electrolytes.[17] In a highly concentrated aqueous electrolyte, the content of free H_2O molecules decreases, leading to less corrosion (dissolution) of electrode materials and a wider electrochemical stability window (ESW) of the electrolyte.[18] For instance, active material's dissolution was significantly suppressed in an AAIB using the concentrated electrolyte [5.8 m $(NH_4)_2SO_4$], exhibiting 72% capacity retention and good coulombic efficiency over 1000 cycles. The ESW was also broadened from 1.34 to 2.39 V upon increasing the electrolyte concentration from 1 to 5.8 m.[18] Recently, Niu *et al.*[19] reported a highly concentrated $NH_4CF_3SO_3$ electrolyte (24 m) for high performance AAIBs. H_2O molecules in the electrolyte were confined by NH_4^+ and $CF_3SO_3^-$ ions in the solvation sheath structure, weakening the water activity, and thus resulting in a large ESW and good cycling stability.

It is known that battery performance is highly associated with the solvation sheath structure of cations.[20] In AAIBs, the high population of anions in a concentrated electrolyte will force them into the solvation sheath of NH_4^+, leading to the formation of a new NH_4^+-anion-H_2O solvation sheath structure.[19] The unique solvated NH_4^+ clusters would adsorb and get de-solvated at the electrolyte–electrode interface, making it the center of charge transfer reactions.[21] Different from other metal

[a]*Department of Chemistry, Northeastern University, 3-11, Wenhua Road, Heping district, Shenyang, 110819, China. E-mail: songyu@mail.neu.edu.cn; xxliu@mail.neu.edu.cn*

[b]*National Frontiers Science Center for Industrial Intelligence and Systems Optimization, Northeastern University, 3-11, Wenhua Road, Heping district, Shenyang, 110819, China*

[c]*Key Laboratory of Data Analytics and Optimization for Smart Industry (Northeastern University), Ministry of Education, 3-11, Wenhua Road, Heping district, Shenyang, 110819, China*

[d]*State Key Laboratory of Metastable Materials Science and Technology, Yanshan University, Qinhuangdao, 066004, China. E-mail: jwang6027@ysu.edu.cn*

† Electronic supplementary information (ESI) available. See DOI: https://doi.org/10.1039/d3sc05318k

cations, NH_4^+ could interact with H_2O molecules, anions and electrode materials *via* H bonding, constituting unusual energy barriers for NH_4^+ de-solvation and intercalation, resulting in distinct physical and electrochemical properties for ammonium-ion batteries.[22] Though previous reports have studied the solvation sheath structures of NH_4^+ in highly concentrated electrolytes [*i.e.*, $(NH_4)_2SO_4$ and $NH_4CF_3SO_3$],[18,19] the complicated electrolyte–electrode interface processes, including the solvated NH_4^+ adsorption and de-solvation, have never been studied, to the best of our knowledge.

In this work, starting from the concentration of electrolyte, we discussed how various concentrations of ammonium acetate (CH_3COONH_4) electrolytes led to different electrochemical performances of an electrochemically activated Co–Ni double hydroxide material (A-CoNi DH). Electrochemical and spectroscopic studies combined with theoretical simulations indicated that the enhanced NH_4^+ storage performance in 15 m CH_3COONH_4 electrolyte was mainly due to the facilitated adsorption/de-solvation processes of the unique solvated NH_4^+ on the electrode surface. Compared to the diluted electrolyte (1 m CH_3COONH_4), the solvated NH_4^+ exhibited stronger adsorption on the electrode surface in the concentrated electrolyte. In addition, a partial de-solvation model was also proposed to demonstrate an energy favorable de-solvation process in the highly concentrated CH_3COONH_4 electrolyte. To illustrate the practical application of the highly concentrated electrolyte, an ammonium-ion hybrid battery [Zn|15 m CH_3COONH_4 + 2 m $Zn(CH_3COO)_2$|A-CoNi DH] was assembled and delivered a high energy density of 368 W h $kg_{(cathode)}^{-1}$, which is better than those of the assembled Zn-ion battery [Zn|2 m $Zn(CH_3COO)_2$|A-CoNi DH] and other reported ammonium-based batteries, indicating the superiority of the highly concentrated CH_3COONH_4 electrolyte and the hybrid ammonium-ion battery design.

Results and discussion

Electrochemistry of A-CoNi DH in CH_3COONH_4 electrolytes with different concentrations

As a study prototype, an electrochemically activated Co–Ni double hydroxide (A-CoNi DH) was deposited on a 3D exfoliated graphite substrate (EG, Fig. S1†) using an electrochemical method reported before.[21] The electrochemical activation strategy could significantly enhance the electrochemical performance of the double hydroxide material (Fig. S2 and S3†).[23,24] Ultrathin nanosheets were uniformly grown on the exfoliated graphene/graphite sheets, forming a hierarchically porous structure (Fig. S4†). The XRD pattern of the A-CoNi DH electrode indicates the amorphous structure of the deposited material (Fig. S5a†). The chemical composition of A-CoNi DH was further characterized *via* energy dispersive X-ray spectroscopy (EDX, Fig. S5b†), Fourier transform infrared spectroscopy (FTIR, Fig. S5c†) and X-ray photoelectron spectroscopy (XPS, Fig. S5d–f†). The results suggest that the possible composition of A-CoNi DH is $Co_{0.78}Ni_{0.22}O_{0.6}(OH)_{1.27}(NO_3)_{0.05}$ (for details please see ESI, Fig. S5†).

To investigate the effect of salt concentration on aqueous NH_4^+ storage, we first tested the electrochemical performance of A-CoNi DH in a three-electrode cell using ammonium acetate electrolytes with different concentrations [1 to 20 mol kg^{-1} (m)], and a saturated calomel electrode (SCE) as the reference electrode. Interestingly, we observe that the concentration of the electrolyte significantly affects the NH_4^+ storage performance of the A-CoNi DH electrode (Fig. 1a). The electrode tested in the concentrated 15 m electrolyte exhibits the optimized performance, delivering a high capacity of 220 mA h g^{-1} at a current density of 0.85 A g^{-1}, which is much higher than that of 172 mA h g^{-1} obtained in 1 m electrolyte (Fig. 1b and S6†). Further increasing the electrolyte concentration to 20 m would lead to capacity decay at a high discharge rate, which could be due to the high viscosity and poor ion conduction in the highly concentrated solution.[25]

The charge storage mechanism of A-CoNi DH in NH_4Ac electrolyte was studied using FTIR and XPS. Upon charging from 0 to 0.8 V *vs.* SCE (Fig. S7†), the intensity of the N–H vibration at 1410 cm^{-1} decreased, and recovered during the subsequent discharging process from 0.8–0 V *vs.* SCE (Fig. 1c). This result indicates that NH_4^+ participated in the charge storage of A-CoNi DH. XPS Co 2p (Fig. 1d) and Ni 2p (Fig. 1e) spectra indicate that both Co and Ni atoms are active sites for charge storage. XPS O 1s spectra of the samples can be fitted into three O containing components, *i.e.*, Co/Ni–O (529.8 eV), Co/Ni–O–H (531.4 eV), and H–O–H (533 eV), as shown in Fig. S8.† Upon discharging from 0.8 to 0 V *vs.* SCE, the content of Co/Ni–O (529.8 eV) slightly decreased, suggesting that a small number of Co/Ni–O species were converted to Co/Ni–O–H due to the inevitable H^+ insertion in aqueous electrolyte. These results suggest that A-CoNi DH experienced a NH_4^+/H^+ co-insertion mechanism, and NH_4^+ is the main charge carrier in this work, which could be due to the highly concentrated NH_4^+ as well as the neutral pH value of the electrolyte. These results are also in accordance with our previous studies.[26,27]

Solvation structure of the concentrated ammonium acetate electrolytes

The above results suggest that the concentration of the electrolyte significantly affects the NH_4^+ storage performance of the A-CoNi DH electrode (Fig. 1a). Therefore, we studied the structural features of the electrolytes with different concentrations. Fig. 2a indicates that the CH_3COONH_4 electrolytes from 1 to 20 m all exhibit good ionic conductivity (higher than 60 mS cm^{-1}), which is higher than those of most of the concentrated aqueous electrolytes, such as 10 m $NH_4CF_3SO_3$ (18 mS cm^{-1}),[19] 30 m $ZnCl_2$ (3 mS cm^{-1}),[28] and 5 M $Zn(ClO_4)_2$ (46 mS cm^{-1}).[29] The high ionic conductivity of the electrolytes ensures fast ion transfer during charge/discharge processes.

In addition to ionic conductivity, the solvation structure of NH_4^+ in these electrolytes plays an important role in the promising electrochemical NH_4^+ storage performances, which is further studied *via* Fourier transform infrared spectroscopy (FTIR), Raman spectroscopy, and theoretical simulation. The specific infrared active bending modes of NH_4^+ and CH_3COO^-

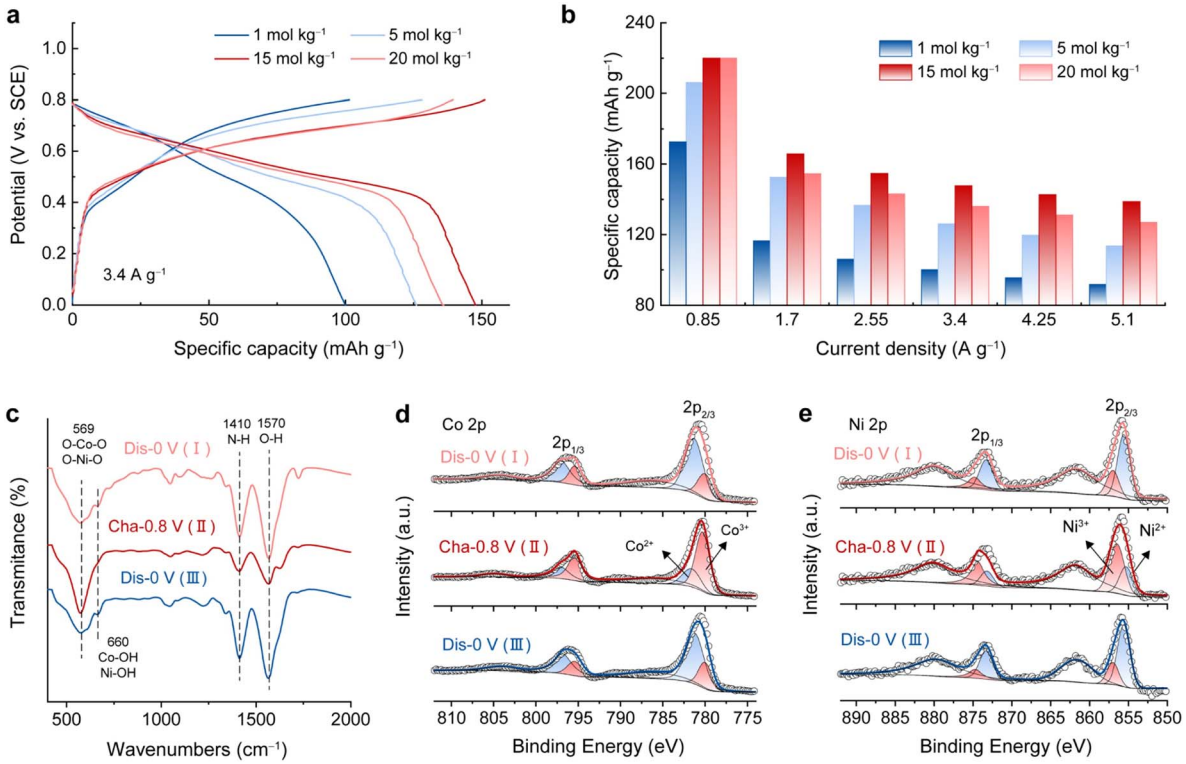

Fig. 1 (a) Galvanostatic charge/discharge curves of the A-CoNi DH electrode in different concentrations of ammonium acetate electrolyte at the current density of 3.4 A g^{-1}. (b) Rate performance of the A-CoNi DH electrode in different electrolytes. (c) FTIR, (d) XPS Co 2p, and (e) XPS Ni 2p spectra of the A-CoNi DH electrode at different states of charge.

were observed at 1414 cm^{-1} and 1552 cm^{-1} for 1 m CH_3COONH_4 electrolyte, respectively (Fig. 2b).[26,30] Interestingly, as the electrolyte concentration increased from 1 to 20 m, the N–H vibration shifts to lower wavenumbers (from 1414 to 1407 cm^{-1}), while the C–O mode moves to higher wavenumbers (from 1552 to 1562 cm^{-1}). These results indicate a strong interaction between NH_4^+ and CH_3COO^- in the electrolytes, and this interaction is strengthened by increasing the concentration of CH_3COONH_4.[31] In order to obtain more band-related information of the overlapped O–H, N–H, and C–H stretching bands at high-wavenumber positions (Fig. 2b), we classified these peaks in Fig. S9† and the results are summarized in Fig. 2c. For O-H components, the higher wavenumber peak at 3620 cm^{-1} can be attributed to the non-hydrogen bond. Two intermediate vibrations at 3515 cm^{-1} and 3350 cm^{-1} are assigned to the weak hydrogen bond, and the lowest wavenumber at 3195 cm^{-1} is labeled as the strong hydrogen bond (Fig. S9†).[32,33] With the increase of CH_3COONH_4 concentration, the proportion of strong and weak hydrogen bonds decreased, and non-hydrogen bonds increased, indicating that the H bond network of the aqueous solution was broken, due to the high proportion of solute in the highly concentrated electrolytes.[19] Besides, the peaks for H bonded NH_4^+ (N–H···O) shifted to lower wavenumbers when the concentration of CH_3COONH_4 increased (Fig. 2b right column and Fig. S9†). In addition to the H bonds between N–H and H_2O, NH_4^+ can also interact with CH_3COO^- upon increasing the CH_3COONH_4 concentration, resulting in the N–H···O peak shift and intensity enhancement. This strong interaction of NH_4^+ with H_2O and CH_3COO^- in the electrolytes plays a crucial role in constructing the solvation structure. In the concentrated electrolytes, CH_3COO^- participates in the construction of the NH_4^+ solvation sheath and expels water molecules. Moreover, as indicated by Raman spectroscopy (Fig. S10†), when the CH_3COONH_4 concentration increased, the characteristic peaks for N–H and C–O shifted, and the water activity reduced, in agreement with the FTIR results.[34,35]

Ab initio molecular dynamics (AIMD) simulation was performed to further study the NH_4^+ solvation structures in different electrolytes. As study prototypes, we selected 1 and 15 m CH_3COONH_4 aqueous solutions to conduct the calculation. The snapshots in Fig. 2d and e show the simulated NH_4^+ solvation structures. In 1 m CH_3COONH_4 electrolyte, NH_4^+ coordinated with five H_2O molecules, and four H_2O molecules bonded with NH_4^+ *via* H bonding, forming a long-lived tetrahedral cage. The fifth H_2O molecule was mobile and flexible exchanging with one of the four H_2O in the tetrahedral cage.[36] The average bond length between the H-bonded water molecules and the central NH_4^+ in the first solvation sheath is 1.88 Å. The radial distribution function (RDF) result suggests that the number of ligands varied in the range of four to six for N–O interaction (NH_4^+-H_2O) in 1 m CH_3COONH_4 solution (Fig. 2f, blue lines). The preferred coordination number was five, which was further confirmed by the density functional theory (DFT) results (Fig. S11†). The larger N–C distance and the low

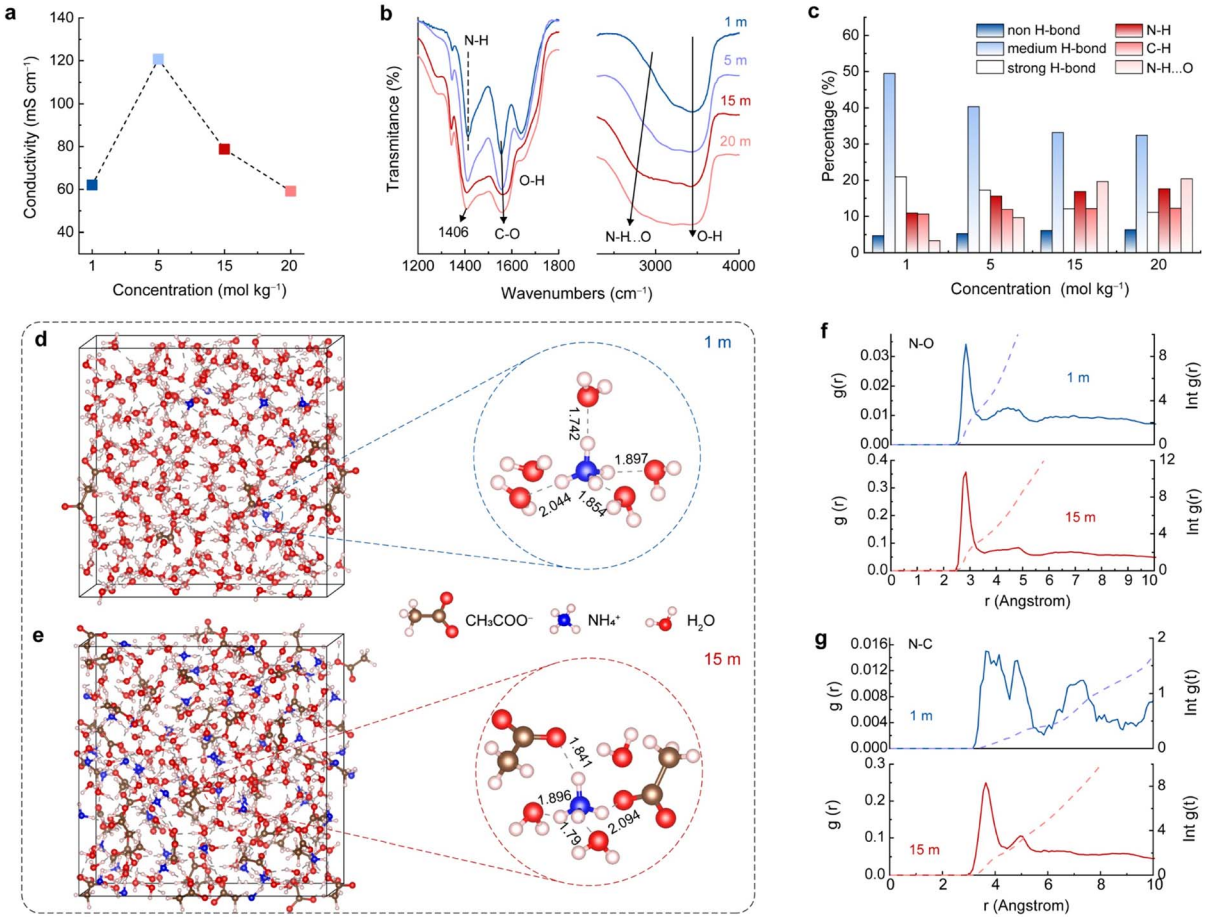

Fig. 2 (a) Electrical conductivity and (b) FTIR spectra of CH_3COONH_4 electrolytes with different concentrations. (c) The corresponding percentage of the chemical bonds summarized in Fig. S9.† (d) and (e) MD simulation. (f) and (g) RDF plots of N–O and N–C, and the corresponding average coordination number of 1 and 15 m CH_3COONH_4 electrolytes.

coordination number as shown in Fig. 2g (blue lines) indicate that CH_3COO^- did not participate in the NH_4^+ solvation sheath in 1 m CH_3COONH_4 solution. By contrast, CH_3COO^- anions tend to supersede partial water molecules and participate in constructing the solvation sheath of the central NH_4^+ in 15 m CH_3COONH_4 electrolyte (Fig. 2e and S12†). RDFs results in Fig. 2f and g (red lines) suggest that one NH_4^+ is coordinated with three H_2O molecules and two CH_3COO^- in the solvation sheath. The simulation snapshot of 15 m CH_3COONH_4 shows that the average distance between NH_4^+ and the H-bonded species is 1.91 Å, which is larger than that in 1 m electrolyte. The increased distance leads to smaller bonding energy and weaker interatomic bonding interaction, facilitating the subsequent de-solvation process during discharging.[37] The above experimental and theoretical results indicate that a higher electrolyte concentration will promote the CH_3COO^- involving in the first solvation sheath of NH_4^+, forming different solvation sheath structures compared with diluted electrolyte. The unique solvated NH_4^+ clusters would adsorb and get de-solvated at the electrolyte–electrode interface, leading to distinct electrochemical features.

Solvation structure–electrochemical performance relationship

Electrochemical impedance spectra (EIS) of the A-CoNi DH electrode were collected in different concentrated NH_4Ac electrolytes (Fig. 3a and S13†). The equivalent series resistances (R_s, Z'-intercept) of the plots are almost the same, indicating that the solution resistances of the NH_4Ac electrolytes have little effect on the electrochemical performance. Yet, the charge transfer resistances (R_{ct}, semicircle diameter) decrease with the increase of electrolyte concentration from 1 to 15 m, and slightly increase when the concentration is higher than 15 m (Fig. S13†). In addition, Fig. 3b and c show that the A-CoNi DH electrode exhibits a much lower redox polarization potential in 15 m CH_3COONH_4 electrolyte, suggesting fast reaction kinetics in the highly concentrated electrolyte. These results explain why the A-CoNi DH electrode shows optimized electrochemical performance in 15 m electrolyte.

In general, the electrode's discharging process usually involves ion diffusion in bulk electrolytes, interfacial behaviors (including ion adsorption and de-solvation) on the electrolyte–electrode interface, and subsequent ionic solid-state migration

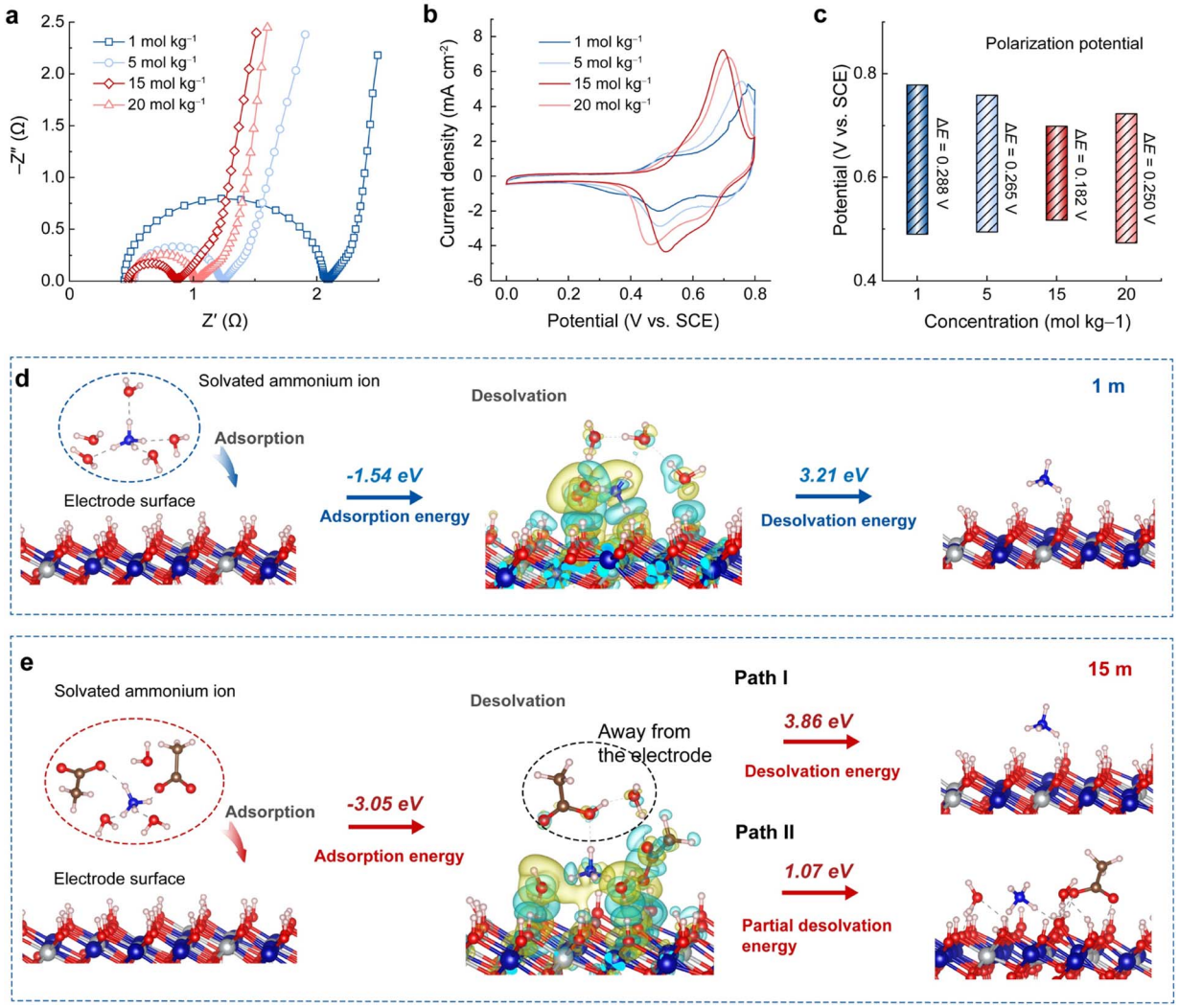

Fig. 3 (a) Nyquist plots of the A-CoNi DH electrode in different concentrated CH_3COONH_4 electrolytes. (b) CV curves of the A-CoNi DH electrodes in different electrolytes at the scan rate of 0.5 mV s^{-1}. (c)The redox polarization potentials of A-CoNi DH's CV curves (b) in different electrolytes. The simulated electrolyte–electrode interface processes upon discharging in (d) 1 m, and (e) 15 m CH_3COONH_4 electrolytes, respectively.

in the electrode matrix. In this work, all the CH_3COONH_4 electrolytes exhibit good ionic conductivity, and the electrolyte concentration will not affect the NH_4^+ solid-state migration in the A-CoNi DH bulk. Therefore, the distinct interfacial processes in different concentrated electrolytes are believed to be the primary factor that affects the electrochemical performances.

To further study the complicated interfacial behavior and disclose the solvation structure-electrochemical performance relationship in aqueous NH_4^+ storage, we present a specific interfacial model that describes the adsorption and de-solvation behaviors of solvated cations (NH_4^+) on the electrode surface. Different from the conventional isolated ion adsorption model,[21] this specific interfacial model could better describe the complicated interaction between cation–anion–solvent and electrode materials. For the diluted electrolyte (1 m CH_3COONH_4, as shown in Fig. 3d), upon discharging, solvated NH_4^+ (optimized from the solvation structure of NH_4^+ in Fig. 2) would attach on the electrode surface, and the adsorption energy is calculated to be −1.54 eV. The differential charge density distribution of the specific adsorption model suggests strong interaction between NH_4^+–H_2O and the electrode material, which demands extra energy as large as 3.21 eV for solvent H_2O molecules de-solvating before NH_4^+ insertion.

By contrast, in the concentrated 15 m electrolyte, the solvated NH_4^+ cluster exhibits a much lower adsorption energy of −3.05 eV compared with that in the diluted electrolyte (Fig. 3e). This can be ascribed to the strong coordination effect of acetate ions that participated in the solvation sheath of NH_4^+ in the concentrated electrolyte, leading to compact interaction between the solvated NH_4^+ and the electrode surface. As a result, a high de-solvation energy of 3.86 eV is required in a complete de-solvation process (Fig. 3e, Path I), which is unfavorable in thermodynamics. However, it is noticed that the solvation structure of NH_4^+ in 15 m

electrolyte is loose due to the large volume of CH_3COO^-, which inspires us to propose a partial de-solvation process. DFT calculations were performed to further study this process. The partial de-solvation model (Fig. 3e, Path II) reveals that the solvated NH_4^+ loses one CH_3COO^- and one H_2O molecule away from the electrode surface and the interaction between NH_4^+ and the H_2O/CH_3COO^- attached on the electrode surface is broken, demanding only 1.07 eV in energy, which is less than that in the complete de-solvation pathway I. As shown in the model, the strong H bonding between the left H_2O/CH_3COO^- and the hydroxide electrode remains (gray dashed lines). These surface adsorbed H_2O and CH_3COO^- will be stable (in the form of O···H–O–metal) even after NH_4^+ insertion. As shown in Fig. S14,† after discharging, the electrode's XPS C 1s signal at higher binding energy (288∼291 eV for $-COO^-$) was significantly enhanced compared with that of the pristine electrode. Another advantage of the partial de-solvation model is that the NH_4^+ is closer to the electrode surface due to the surface re-arrangement, which is beneficial for the insertion into the electrode material. Therefore, in the highly concentrated electrolyte, acetate anions would participate in the solvation structure of NH_4^+, and therefore improve the adsorption thermodynamics of the solvated NH_4^+ on the electrode surface. The proposed partial de-solvation model also provides an energy favorable NH_4^+ de-solvation process with low energy cost. All these features lead to the decreased charge transfer resistance and electrochemical polarization, and therefore make the highly concentrated electrolyte attractive in aqueous NH_4^+ storage.

High-performance NH_4^+-ion hybrid battery

To test the practical application of the highly concentrated CH_3COONH_4 electrolyte, an ammonium ion hybrid battery was assembled using A-CoNi DH as the cathode and a piece of zinc foil as the anode (Fig. 4a). To make sure that there are enough Zn^{2+} ions in the electrolyte for Zn deposition, a small amount of anhydrous $Zn(CH_3COO)_2$ was added into 15 m CH_3COONH_4 electrolyte to form the optimized hybrid electrolyte, *i.e.*, 15 m CH_3COONH_4 + 2 m $Zn(CH_3COO)_2$ (Fig. S15†). SEM, XRD, XPS and EDX results suggest that the Zn^{2+} in the hybrid electrolyte did not participate the charge storage of the A-CoNi DH cathode (Fig. S16–S19†). Theoretical simulation was performed to further study the NH_4^+ solvation structures as well as the cation diffusion barrier (Tables S1 and S2†) in the hybrid electrolyte (Fig. 4b). The snapshot of the solvated NH_4^+ indicates that the small amount of Zn^{2+} additives in the hybrid electrolyte did not change the solvation structure of NH_4^+. In addition, the calculated adsorption energy of NH_4^+ (−0.08 eV) on the electrode surface is lower than that of Zn^{2+} (+0.65 eV), suggesting the favorable thermodynamic adsorption of NH_4^+ on A-CoNi DH. These results explain why Zn^{2+} did not participate in the charge storage of A-CoNi DH in the hybrid electrolyte. The possible chemical reactions occurring in the hybrid device are summarized as below:

Cathode:

$$Co_{0.78}Ni_{0.22}O_{0.6}(OH)_{1.27}(NO_3)_{0.05} + NH_4^+ + e^- \leftrightarrow (NH_4)Co_{0.78}Ni_{0.22}O_{0.6}(OH)_{1.27}(NO_3)_{0.05}$$

Anode:

$$1/2Zn \leftrightarrow 1/2Zn^{2+} + e^-$$

Overall:

$$Co_{0.78}Ni_{0.22}O_{0.6}(OH)_{1.27}(NO_3)_{0.05} + NH_4^+ + 1/2Zn \leftrightarrow (NH_4)Co_{0.78}Ni_{0.22}O_{0.6}(OH)_{1.27}(NO_3)_{0.05} + 1/2Zn^{2+}$$

To demonstrate the superiority of this hybrid electrolyte design, we also tested the electrochemical performance of a Zn-ion battery for comparison, using the 2 m $Zn(CH_3COO)_2$ electrolyte, A-CoNi DH cathode and Zn anode, respectively. The hybrid NH_4^+ ion battery exhibited a high capacity of 216 mA h g^{-1} at current density of 1 A g^{-1} and 116 mA h g^{-1} at 10 A g^{-1}, which are higher than those (193.7 mA h g^{-1}@1 A g^{-1} and 0.2 mA h g^{-1}@10 A g^{-1}) of the Zn-ion battery using 2 m $Zn(CH_3COO)_2$ electrolyte (Fig. 4c, d and S20†). Importantly, the charge/discharge curves and the corresponding differential capacity profile of the hybrid device display a high discharge plateau around 1.76 V (Fig. 4c and S21†), because of the high NH_4^+ insertion potential *vs.* Zn^{2+}/Zn. This value is much higher than that of the assembled Zn-ion battery in this work. The electrochemical impedance spectra (EIS) of the A-CoNi DH electrode in the hybrid electrolyte and 2 m $Zn(CH_3COO)_2$ electrolyte were collected and are shown in Fig. 4e. The concentrated hybrid electrolyte exhibits a smaller equivalent series resistance (R_s, the intercept of the x-axis) than 2 m $Zn(CH_3COO)_2$, indicating the higher electrical conductivity of the hybrid electrolyte. In addition, the electrode in the hybrid electrolyte also shows a much smaller charge transfer resistance (R_{ct}) of 0.3 Ω, which can well explain the superior rate performance of the hybrid device. This hybrid battery can deliver a good capacity retention of 75% after 2000 charge–discharge cycles at the current density of 10 A g^{-1} (Fig. 4f). The capacity degradation could be due to the slight dissolution of the active materials in the electrolyte during the charge/discharge processes (Fig. S22†). The average discharge voltage *vs.* the discharge capacity of the hybrid NH_4^+-ion battery with other aqueous batteries, including aqueous NH_4^+-ion and Zn^{2+}-ion batteries, is shown in Fig. 4g and Table S3.† The hybrid battery exhibited a high average voltage of about 1.7 V and a relatively good gravimetric capacity of 216 mA h g^{-1}, which are higher than or comparable with those of other aqueous NH_4^+ and Zn^{2+}-ion batteries.[8,9,15,38–50] Therefore, the hybrid device exhibits a high energy density of 368 W h $kg_{(cathode)}^{-1}$ at a power density of 1703 and 192 W h $kg_{(cathode)}^{-1}$ at an excellent power density of 16 531 W kg^{-1}, outperforming most of the reported aqueous batteries (Fig. 4h and Table S4†).[8,15,38–43,49,51]

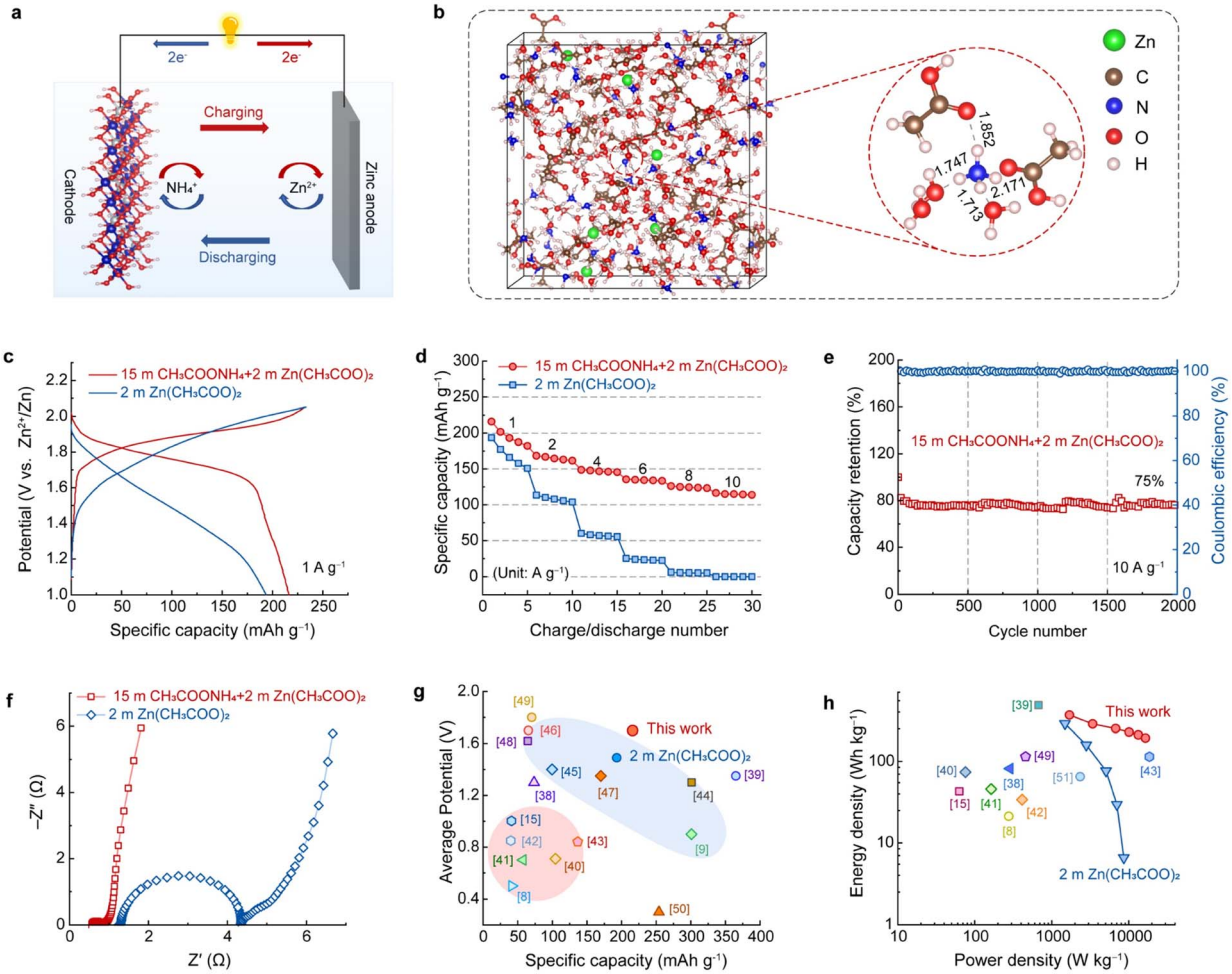

Fig. 4 (a) Schematic illustration of a hybrid ammonium ion battery. (b) MD simulation of 15 m CH_3COONH_4 + 2 m $Zn(CH_3COO)_2$ electrolyte. (c) Galvanostatic charge/discharge curves, and (d) rate performance of the hybrid NH_4^+-ion battery and the assembled Zn^{2+}-ion battery. (e) Nyquist plots of the A-CoNi DH electrode in 15 m CH_3COONH_4 + 2 m $Zn(CH_3COO)_2$ and 2 m $Zn(CH_3COO)_2$ electrolytes. (f) Cycling stability of the hybrid device at the current density of 10 A g^{-1}. (g) The average potential *vs.* discharge capacity, and (h) Ragone plots of the hybrid battery and recently reported aqueous batteries for comparison.

Conclusions

In summary, we fabricated an electrochemically activated CoNi hydroxide material and tested the electrochemical performances of the electrode in different concentrated ammonium acetate (CH_3COONH_4, from 1 to 20 m) electrolytes. The A-CoNi DH electrode exhibited the optimized electrochemical performance in 15 m CH_3COONH_4 electrolyte. The theoretical calculation, and spectroscopic and electrochemical studies established a direct correlation between the NH_4^+ solvation-sheath structure and the electrode's performances in different concentrated electrolytes. In 15 m electrolyte, acetate will replace water molecules and participate in the NH_4^+ solvation sheath, leading to a stronger specific adsorption between the solvated NH_4^+ and the A-CoNi DH electrode. In addition, a partial de-solvation model was proposed, in which the interaction between NH_4^+ and the surrounding solvated molecules, *i.e.*, acetate and water, was broken. The electrode surface adsorbed acetate and water molecules do not necessarily de-solvated into the electrolytes, but bound to the hydroxide on the electrode surface, leading to a low energy cost process. To illustrate the practical application of the highly concentrated electrolyte, an ammonium-ion hybrid battery [Zn|15 m CH_3COONH_4 + 2 m $Zn(CH_3COO)_2$|A-CoNi DH] was assembled, which provided a high energy density of 368 W h kg(cathode)$^{-1}$, a high working voltage of 1.7 V and good rate performance, outperforming most of the reported aqueous batteries. This work provides new understanding about the electrode–electrolyte interface processes in differently concentrated NH_4^+ based electrolytes, opening a viable route to the development of promising NH_4^+-ion batteries, which may also be extended to other aqueous batteries.

Author contributions

J. M., Y. S., and J. W. conceived the project and designed this work. The experiment was performed by J. M. under the guidance of Y. S. and X.-X. L. with the help of P. H., C. L., M. L. and Y. L. carried out the SEM and FTIR tests. J. W. carried out the DFT

calculations. J. M. and Y. S. wrote the manuscript. All authors discussed the results and commented on the manuscript.

Conflicts of interest

There are no conflicts to declare.

Acknowledgements

Y. S. acknowledges the financial support from the Fundamental Research Funds for the Central Universities (Grant No. N2205003) and Natural Science Foundation of Liaoning Province (no. 2023-MS-080). J. W. is thankful for the financial support from the Hebei Science Foundation (no. B2021203016 and E2021203005), Hebei provincial Department of Human Resources and Social Security (C20210503) and Hebei Education department (BJ2021042). The authors thank Y. Dong from the Analytical and Testing Center of Northeastern University for data acquisition.

References

1 S. Dong, W. Shin, H. Jiang, X. Wu, Z. Li, J. Holoubek, W. F. Stickle, B. Key, C. Liu, J. Lu, P. A. Greaney, X. Zhang and X. Ji, Ultra-fast NH_4^+ storage: strong H bonding between NH_4^+ and bi-layered V_2O_5, *Chem*, 2019, **5**, 1537–1551.

2 T. H. Lu, C. Zeng, H. Zhang, X. Shi, Y. Yu and X. Lu, Valence engineering enhancing NH_4^+ storage capacity of manganese oxides, *Small*, 2023, **19**, 2206727.

3 L. Han, J. Luo, R. Zhang, W. Gong, L. Chen, F. Liu, Y. Ling, Y. Dong, Z. Yong, Y. Zhang, L. Wei, X. Zhang, Q. Zhang and Q. Li, Arrayed heterostructures of MoS_2 nanosheets anchored TiN nanowires as efficient pseudocapacitive anodes for fiber-shaped ammonium-ion asymmetric supercapacitors, *ACS Nano*, 2022, **16**, 14951–14962.

4 R. Zheng, Y. Li, H. Yu, X. Zhang, D. Yang, L. Yan, Y. Li, J. Shu and B. L. Su, Ammonium ion batteries: material, electrochemistry and strategy, *Angew. Chem., Int. Ed.*, 2023, **62**, e202301629.

5 Q. Chen, M. Song, X. Zhang, J. Zhang, G. Hou and Y. Tang, Ammonium ion pre-intercalation stabilized tunnel h-WO_3 for fast NH_4^+ storage, *J. Mater. Chem. A*, 2022, **10**, 15614–15622.

6 S. F. Kuchena and Y. Wang, V_2O_5 intercalated with polyaniline for improved kinetics in aqueous ammonium-ion batteries, *Electrochim. Acta*, 2022, **425**, 140751.

7 Y. Wu, S. Dong, N. Lv, Z. Xu, R. Ren, G. Zhu, B. Huang, Y. Zhang and X. Dong, Unlocking the high capacity ammonium-ion storage in defective vanadium dioxide, *Small*, 2022, **18**, 2204888.

8 G. Liang, Y. Wang, Z. Huang, F. Mo, X. Li, Q. Yang, D. Wang, H. Li, S. Chen and C. Zhi, Initiating hexagonal MoO_3 for superb-stable and fast NH_4^+ storage based on hydrogen bond chemistry, *Adv. Mater.*, 2020, **32**, 1907802.

9 D. Yu, Z. Wei, X. Zhang, Y. Zeng, C. Wang, G. Chen, Z. X. Shen and F. Du, Boosting Zn^{2+} and NH_4^+ storage in aqueous media *via in situ* electrochemical induced VS_2/VO_x heterostructures, *Adv. Funct. Mater.*, 2020, **31**, 2008743.

10 F. Ye, R. Pang, C. Lu, Q. Liu, Y. Wu, R. Ma and L. Hu, Reversible ammonium ion intercalation/de-intercalation with crystal water promotion effect in layered $VOPO_4 \cdot 2H_2O$, *Angew. Chem., Int. Ed.*, 2023, **62**, e202303480.

11 S. Zhang, K. Zhu, Y. Gao and D. Cao, A long cycle stability and high rate performance organic anode for rechargeable aqueous ammonium-ion battery, *ACS Energy Lett.*, 2023, **8**, 889–897.

12 H. Zhang, Y. Tian, W. Wang, Z. Jian and W. Chen, Organic ammonium ion battery: A new strategy for a nonmetallic ion energy storage system, *Angew. Chem., Int. Ed.*, 2022, **61**, e202204351.

13 S. Li, M. Xia, C. Xiao, X. Zhang, H. Yu, L. Zhang and J. Shu, Common ion effect enhanced prussian blue analogues for aqueous ammonium ion storage, *Dalton Trans.*, 2021, **50**, 6520–6527.

14 H. Yu, L. Fan, H. Yan, C. Deng, L. Yan, J. Shu and Z. B. Wang, Optimizing NH_4^+ storage capability of nickel ferrocyanide by regulating coordination anion in aqueous electrolytes, *ChemElectroChem*, 2022, **9**, e202200492.

15 X. Wu, Y. Qi, J. J. Hong, Z. Li, A. S. Hernandez and X. Ji, Rocking-chair ammonium-ion battery: A highly reversible aqueous energy storage system, *Angew. Chem., Int. Ed.*, 2017, **56**, 13026–13030.

16 X. Zhang, M. Xia, T. Liu, N. Peng, H. Yu, R. Zheng, L. Zhang, M. Shui and J. Shu, Copper hexacyanoferrate as ultra-high rate host for aqueous ammonium ion storage, *Chem. Eng. J.*, 2021, **421**, 127767.

17 F. Wang, O. Borodin, T. Gao, X. Fan, W. Sun, F. Han, A. Faraone, J. A. Dura, K. Xu and C. Wang, Highly reversible zinc metal anode for aqueous batteries, *Nat. Mater.*, 2018, **17**, 543–549.

18 J. Han, M. Zarrabeitia, A. Mariani, M. Kuenzel, A. Mullaliu, A. Varzi and S. Passerini, Concentrated electrolytes enabling stable aqueous ammonium-ion batteries, *Adv. Mater.*, 2022, **34**, 2201877.

19 L. Du, S. Bi, M. Yang, Z. Tie, M. Zhang and Z. Niu, Coupling dual metal active sites and low-solvation architecture toward high-performance aqueous ammonium-ion batteries, *Proc. Natl. Acad. Sci. U.S.A.*, 2022, **119**, e2214545119.

20 Z. Tian, J. Yin, T. Guo, Z. Zhao, Y. Zhu, Y. Wang, J. Yin, Y. Zou, Y. Lei, J. Ming, O. Bakr, O. F. Mohammed and H. N. Alshareef, A sustainable NH_4^+ ion battery by electrolyte engineering, *Angew. Chem., Int. Ed.*, 2022, **61**, e202213757.

21 M. Huang, Q. He, J. Wang, X. Liu, F. Xiong, Y. Liu, R. Guo, Y. Zhao, J. Yang and L. Mai, NH_4^+ deprotonation at interfaces induced reversible H_3O^+/NH_4^+ co-insertion/extraction, *Angew. Chem., Int. Ed.*, 2023, **62**, e202218922.

22 Z. Tian, V. S. Kale, Y. Wang, S. Kandambeth, J. Czaban-Jóźwiak, O. Shekhah, M. Eddaoudi and H. N. Alshareef, High-capacity NH_4^+ charge storage in covalent organic frameworks, *J. Am. Chem. Soc.*, 2021, **143**, 19178–19186.

23 J. Meng, Y. Song, Z. Qin, Z. Wang, X. Mu, J. Wang and X. X. Liu, Cobalt-nickel double hydroxide toward mild

aqueous zinc-ion batteries, *Adv. Funct. Mater.*, 2022, **32**, 2204026.

24 C. Liu, M. Li, J. Meng, P. Hei, J. Wang, Y. Song and X. X. Liu, Electrochemical storage of ammonium *versus* metal ions in bimetallic hydroxide for sustainable aqueous batteries, *Adv. Funct. Mater.*, 2023, DOI: 10.1002/adfm.202310437.

25 S. Gao, B. Li, H. Tan, F. Xia, O. Dahunsi, W. Xu, Y. Liu, R. Wang and Y. Cheng, High-energy and stable subfreezing aqueous Zn-MnO_2 batteries with selective and pseudocapacitive zn-ion insertion in MnO_2, *Adv. Mater.*, 2022, **34**, 2201510.

26 D. Yang, Y. Song, M. Y. Zhang, Z. Qin, J. Liu and X. X. Liu, Solid-liquid interfacial coordination chemistry enables high-capacity ammonium storage in amorphous manganese phosphate, *Angew. Chem., Int. Ed.*, 2022, **61**, e202207711.

27 Q. Pan, H. Peng, Y. Song, J. Meng, C. Liu and X. X. Liu, Electrochemically activated nickel-cobalt double hydroxide for aqueous ammonium-zinc hybrid battery, *Nano Res.*, 2023, **16**, 2495–2501.

28 L. Li, S. Liu, W. Liu, D. Ba, W. Liu, Q. Gui, Y. Chen, Z. Hu, Y. Li and J. Liu, Electrolyte concentration regulation boosting zinc storage stability of high-capacity $K_{0.486}V_2O_5$ cathode for bendable quasi-solid-state zinc ion batteries, *Nano-Micro Lett.*, 2021, 13.

29 G. Yang, J. Huang, X. Wan, B. Liu, Y. Zhu, J. Wang, O. Fontaine, S. Luo, P. Hiralal, Y. Guo and H. Zhou, An aqueous zinc-ion battery working at −50°C enabled by low-concentration perchlorate-based chaotropic salt electrolyte, *EcoMat*, 2022, **4**, e12165.

30 J. Wu, X. Li, W. Shi, P. Ling, Y. Sun, X. Jiao, S. Gao, L. Liang, J. Xu, W. Yan, C. Wang and Y. Xie, Efficient visible-light-driven CO_2 reduction mediated by defect-engineered BiOBr atomic layers, *Angew. Chem., Int. Ed.*, 2018, **130**, 8855–8859.

31 S. Liu, J. Mao, W. K. Pang, J. Vongsvivut, X. Zeng, L. Thomsen, Y. Wang, J. Liu, D. Li and Z. Guo, Tuning the electrolyte solvation structure to suppress cathode dissolution, water reactivity, and zn dendrite growth in zinc-ion batteries, *Adv. Funct. Mater.*, 2021, **31**, 2104281.

32 Q. Li, C. Yang, J. Zhang, X. Ji, J. Xu, X. He, L. Chen, S. Hou, J. Uddin, D. Addison, D. Sun, C. Wang and F. Wang, Controlling intermolecular interaction and interphase chemistry enabled sustainable water-tolerance $LiMn_2O_4$||$Li_4Ti_5O_{12}$ batteries, *Angew. Chem., Int. Ed.*, 2022, **61**, e202214126.

33 Y. Chen, Y.-H. Zhang and L.-J. Zhao, ATR-FTIR spectroscopic studies on aqueous $LiClO_4$, $NaClO_4$, and $Mg(ClO_4)_2$ solutions, *Phys. Chem. Chem. Phys.*, 2004, **6**, 537–542.

34 H. Bhatt, C. Murli, A. K. Mishra, A. K. Verma, N. Garg, M. N. Deo, R. Chitra and S. M. Sharma, Hydrogen bond symmetrization in glycinium oxalate under pressure, *J. Phys. Chem. B*, 2016, **120**, 851–859.

35 J. L. Dong, X. H. Li, L. J. Zhao, H. S. Xiao, F. Wang, X. Guo and Y. H. Zhang, Raman observation of the interactions between NH_4^+, SO_4^{2-}, and H_2O in supersaturated $(NH_4)_2SO_4$ droplets, *J. Phys. Chem. B*, 2007, **111**, 12170–12176.

36 F. Brugé, M. Bernasconi and M. Parrinello, Ab initio simulation of rotational dynamics of solvated ammonium ion in water, *J. Am. Chem. Soc.*, 1999, **121**, 10883–10888.

37 M. Li, Y. Zhang, J. Hu, X. Wang, J. Zhu, C. Niu, C. Han and L. Mai, Universal multifunctional hydrogen bond network construction strategy for enhanced aqueous Zn^{2+}/proton hybrid batteries, *Nano Energy*, 2022, **100**, 107539.

38 C. Li, D. Zhang, F. Ma, T. Ma, J. Wang, Y. Chen, Y. Zhu, L. Fu, Y. Wu and W. Huang, A high-rate and long-life aqueous rechargeable ammonium zinc hybrid battery, *ChemSusChem*, 2019, **12**, 3732–3736.

39 S. Wang, Z. Yuan, X. Zhang, S. Bi, Z. Zhou, J. Tian, Q. Zhang and Z. Niu, Non-metal ion co-insertion chemistry in aqueous Zn/MnO_2 batteries, *Angew. Chem., Int. Ed.*, 2021, **60**, 7056–7060.

40 X. Mu, Y. Song, Z. Qin, J. Meng, Z. Wang and X. X. Liu, Core-shell structural vanadium oxide/polypyrrole anode for aqueous ammonium-ion batteries, *Chem. Eng. J.*, 2023, **453**, 139575.

41 Q. Liu, F. Ye, K. Guan, Y. Yang, H. Dong, Y. Wu, Z. Tang and L. Hu, MnAl layered double hydroxides: a robust host for aqueous ammonium-ion storage with stable plateau and high capacity, *Adv. Energy Mater.*, 2022, **13**, 2202908.

42 Y. Z. Zhang, J. Liang, Z. Huang, Q. Wang, G. Zhu, S. Dong, H. Liang and X. Dong, Ionically conductive tunnels in h-WO_3 enable high-rate NH_4^+ storage, *Adv. Sci.*, 2022, **9**, 2105158.

43 G. Zhou, X. An, C. Zhou, Y. Wu, Y.-E. Miao and T. Liu, Highly porous electroactive polyimide-based nanofibrous composite anode for all-organic aqueous ammonium dual-ion batteries, *Compos. Commun.*, 2020, **22**, 100519.

44 B. Wu, G. Zhang, M. Yan, T. Xiong, P. He, L. He, X. Xu and L. Mai, Graphene scroll-coated α-MnO_2 nanowires as high-performance cathode materials for aqueous zn-ion battery, *Small*, 2018, **14**, 1703850.

45 Y. Zeng, X. F. Lu, S. L. Zhang, D. Luan, S. Li and X. W. Lou, Construction of Co-Mn prussian blue analog hollow spheres for efficient aqueous zn-ion batteries, *Angew. Chem., Int. Ed.*, 2021, **60**, 22189–22194.

46 L. Zhang, L. Chen, X. Zhou and Z. Liu, Towards high-voltage aqueous metal-ion batteries beyond 1.5 V: the zinc/zinc hexacyanoferrate system, *Adv. Energy Mater.*, 2015, **5**, 1400930.

47 H. Y. Shi, Y. Song, Z. Qin, C. Li, D. Guo, X. X. Liu and X. Sun, Inhibiting $VOPO_4 \cdot xH_2O$ decomposition and dissolution in rechargeable aqueous zinc batteries to promote voltage and capacity stabilities, *Angew. Chem., Int. Ed.*, 2019, **58**, 16057–16061.

48 W. Li, K. Wang, S. Cheng and K. Jiang, A long-life aqueous zn-ion battery based on $Na_3V_2(PO_4)_2F_3$ cathode, *Energy Storage Mater.*, 2018, **15**, 14–21.

49 C. Li, J. Wu, F. Ma, Y. Chen, L. Fu, Y. Zhu, Y. Zhang, P. Wang, Y. Wu and W. Huang, High-rate and high-voltage aqueous rechargeable zinc ammonium hybrid battery from selective cation intercalation cathode, *ACS Appl. Energy Mater.*, 2019, **2**, 6984–6989.

50 C. Huang, Y. Liu, J. Li, Z. Miao, X. Cai, Z. Wu, H. Yu, L. Yan, L. Zhang and J. Shu, Organic interlayer engineering of TiS_2 for enhanced aqueous Zn ions storage, *J. Mater. Sci. Technol.*, 2023, **140**, 135–141.

51 X. Wen, J. Lou, K. Xiang, W. Zhou, C. Zhang and H. Chen, High-performance monoclinic WO_3 nanospheres with the novel NH_4^+ diffusion behaviors for aqueous ammonium-ion batteries, *Chem. Eng. J.*, 2023, **458**, 141381.